OBSERVATIONS AND MODELS OF THE GENERAL CIRCULATION OF JUPITER AND SATURN

AGUSTÍN SÁNCHEZ-LAVEGA, RICARDO HUESO, SANTIAGO PÉREZ-HOYOS
Departamento de Física Aplicada I, Escuela Superior de Ingenieros, Universidad del País Vasco, E-48013 Bilbao, SPAIN
ENRIQUE GARCÍA-MELENDO
Esteve Duran Observatory Foundation, Seva, E-08553 Barcelona, SPAIN
JOSE FÉLIX ROJAS
Departamento de Física Aplicada I, Escuela Universitaria de Ingeniería Técnica Industrial, Universidad del País Vasco, E-48012 Bilbao, SPAIN

Abstract: We review our current understanding of the general circulation at cloud top levels in the atmospheres of the giant planets Jupiter and Saturn.

1 Introduction

The giant planets of our Solar System are divided according to their size and properties in two groups: "gas giants" (Jupiter and Saturn, equatorial radius 71,300 km and 60,330 km respectively) and "icy giants" (Uranus and Neptune, radius $\sim$ 25,000 km). Their aspect in images taken at wavelengths ranging from the ultraviolet to the near infrared, is dominated by the diffuse reflection of the sunlight (scattering and absorption) on gases and particles (clouds and hazes located typically at pressure levels $\sim 0.3 - 2$ bar) (Figure 1). Tracking cloud elements along a given temporal interval allows to measure atmospheric motions at these levels. Wind velocities are measured relative to the rotation of the magnetic field, which is assumed to be that of the planet itself (the magnetic field is rooted to the deep interior). Ground-based and spacecraft observations have revealed that the gas giant circulation is dominated by a system of zonal jets, i.e. directed along the parallels, and alternating their direction with latitude. There are 8 and 4 eastward jets per hemisphere in Jupiter and Saturn respectively. A conspicuous characteristic is the existence of a broad in latitude eastward equatorial jet with peak velocities of $\sim 150\ ms^{-1}$ in Jupiter and $\sim 475\ ms^{-1}$ in Saturn (the velocities are taken positive for motions in the eastward direction). On the contrary, the "icy giants" show an eastward hemispheric jet and

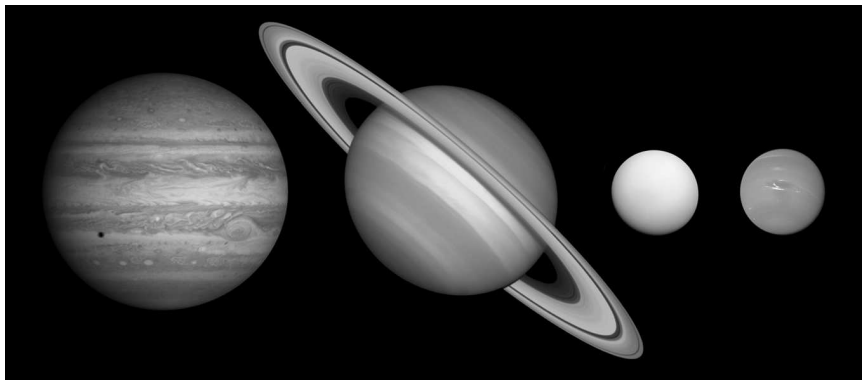

Figure 1: Visual aspect to scale of Jupiter, Saturn, Uranus and Neptune (from left to right) as imaged by the HST (Jupiter) and Voyager spacecrafts (rest). Credit: NASA-JPL.

a broad westward equatorial jet that amounts to - 400 ms^{-1} on Neptune (see Figure 2). At present, there is no accepted theory to explain the nature of these motions [1], and the models presented so far are on a rudimentary stage [2]. This represents a major challenge to a wide community formed by planetary scientists, astrophysicists and meteorologists. Here we will summarize the "state of the art" of this problem, from both observations and theory, but focusing on the gas giant planets for which we have much more data. The interest in these planets has largely grown in the last years in view of their similarities with the recently discovered giant extrasolar planets.

2 Gas giant planets: basic properties

In Table 1 we give the basic properties of the planets that are relevant for the general circulation models including the best studied extrasolar planet, HD 209458b that pertains to the so called family of "hot Jupiters" [3]. The most remarkable physical aspects of the giant planets are [1, 2, 3]:

- Their size is $\sim$ 10 times that of the Earth.

- They have high angular rotation velocity (periods $\sim$ 10 hr), except for the close-in extrasolar "hot Jupiters", assumed to be spin-orbit locked (periods $\sim$ 3 - 4 days).

- The atmospheres of the giants are deep, since they occupy an important fraction of the planetary radius, and frictionless when compared to the Earth due to the lack of a solid surface.

- They have a significant internal energy source coming mainly from the slow cool-

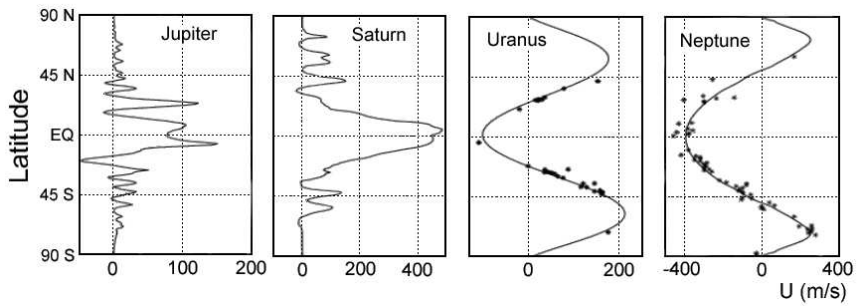

Figure 2: Comparison of the latitudinal zonal wind velocity profiles at cloud level in the giant and icy planets. Adapted from [4].

ing of the planet, i. e. they are releasing the heat accumulated during its formation. This energy is radiated as a black body with peak emission in the infrared (Figure 3). The internal energy source is a factor ~ 1.7 of the absorbed sunlight radiation for Jupiter and Saturn but it is insignificant at cloud levels in the "hot Jupiters" when compared to the strong stellar flux. Whereas the sunlight absorption depends strongly on the sub-solar latitude (due to the planetary axis tilt), the emitted energy is independent of latitude. The total thermal energy available in Jupiter and Saturn is a factor $\sim 1/25$ and $1/100$ respectively of that received on the Earth. Paradoxically the winds are ten times stronger.

- These planets are fully cloud covered. The clouds and aerosol optical depths are high enough to block the visible incident solar radiation in the upper few atmospheric bars. The clouds also partially block the emergent infrared radiation from the interior

Planet	R_P(km)	X	T(hr)	F_{int}(Wm^{-2})	F_{star}(Wm^{-2})
Jupiter	71400	0.8	9.925	5.44	13.6
Saturn	60330	0.5	10.66	2.01	4.6
HD 209458b	96400	~ 0.5	67.67	3	1.2×10^6

Table 1: Main properties of the giant planets. *Notes:* $X = (Rp - D)/Rp$, where D is the thickness of the H_2 molecular layer, T = rotation period, F_{int} = internal energy flux, F_{star} = external (stellar energy flux). For these planets, the range of values for the adimensional numbers in the atmosphere (they depend on altitude) are: $Pr = 10^{-4} - 1$; $Ra = 10^{12} - 10^{24}$; $E = 10^{-10} - 10^{-15}$; $Re = 10^9 - 10^{11}$.

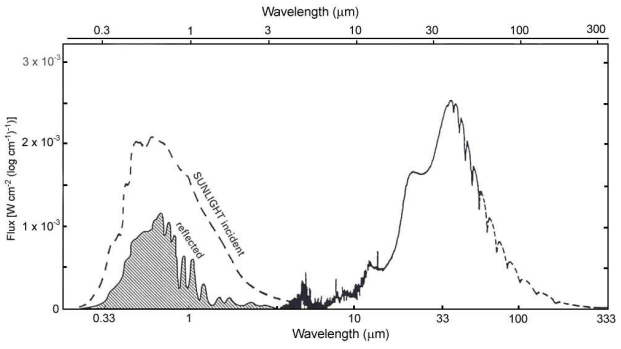

Figure 3: Jupiter's spectrum from the ultraviolet to submm wavelengths. The left part shows the received and absorbed solar radiation (shaded area) and the right part the emitted infrared radiation, escaping from the interior. Adapted from [5].

(see Figure 4).

- Thermodynamic effects related to latent heat release from cloud condensation and, to a minor extent, ortho-para conversion of molecular hydrogen could have an important influence on global dynamics in the upper atmosphere.

- The poorly known internal structure and composition of these planets could have a significant role on the observed motions (Figure 5). Among them, the magnetic and friction effects in the metallic-molecular transition region, and the existence of opacity sources could be important.

In view of the preceding points, the basic unresolved questions are: How is the powerful system of zonal jets generated? How does the intense eastward and broad equatorial jet form? How deep do the winds extend into the interior? These questions come down to know how a thermodynamic machine is able to produce the highly energetic jets and their latitudinal distribution employing such low energy sources.

3 Wind velocity measurements

As already mentioned, observations of the motions of individual cloud features in a given temporal interval are used to measure the winds, either by cloud tracking or by correlation of the zonal albedo patterns. The pressure level at which these winds are measured is about 0.5 ± 0.2 bar where cloud optical depths ~ 1 to 3 are reached on both planets. High spatial resolution images obtained by means of cameras onboard various spacecrafts have provided the best wind data. In Jupiter these images were obtained by the Voyager 1 and 2 in 1979 [6, 7], by the Hubble Space Telescope from

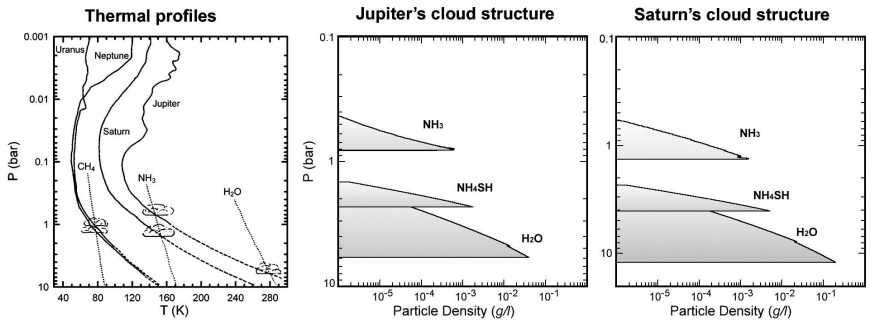

Figure 4: Left: Vertical temperature profiles in the visible part of the four planets. The main composition and altitude of the main clouds are indicated. From [10]. Center and Right: Altitude location and densities of the main clouds in Jupiter and Saturn as calculated from thermochemical models.

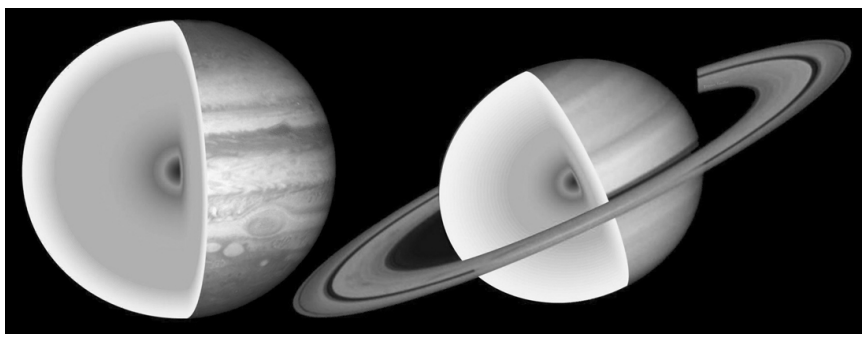

Figure 5: Static models of the internal structure of Jupiter and Saturn. The following regions are expected (from the upper clouds to interior): (a) An hydrogen molecular layer (the atmosphere), (b) A plasma (fluid) metallic hydrogen layer, (c) A central region formed by a coating of "ices" surrounding a central rocky core. The extension of each layer is to scale. Adapted from [11]

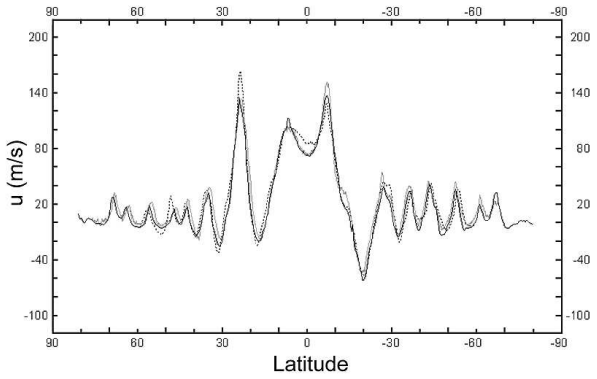

Figure 6: A comparison of different Jupiter's wind profiles as a function of time: Dotted line (Voyagers, 1979) [7]; Continuous gray line, (HST, from 1996 to 2000) [8]; Continuous dark, (Cassini 2000) [9]).

1995 to 2000 [8], by the Cassini Orbiter during its flyby in route to Saturn in 2000 [9], and by the Galileo Orbiter for some particular regions from 1996 to 2002 [12]. The maximum resolution attained in Jupiter is $\sim$ 50 km/pixel. For Saturn the data came from the Voyager 1 and 2 flybies in 1980 and 1981 [13, 14] and from HST from 1994 to 2003 [15, 16, 17, 18], with a maximum resolution $\sim$ 150 km/pixel. The Cassini Orbiter will also provide similarly accurate data during its mission starting in mid-2004.

Measurements of wind velocity vectors are usually affected by different types of errors (e. g. limb fitting of the planet, position determination of the targets and target identification), amounting to values 5 to 10 ms^{-1} for Jupiter and 10-15 ms^{-1} for Saturn. The maximum number of wind vectors measured was $N \sim$ 14,000 for Jupiter and $N \sim$ 2,300 for Saturn. Mean zonal velocities $<u>$ (averaged in longitude) must be retrieved taking into account the local motions related to the particular features present in the flow (vortices, waves, turbulence) [8]. In Figure 6 we compare the mean zonal Jupiter profile as measured in three periods. Although changes in the jets intensity have been detected (for example at 23°N latitude, see below), the long-term ground-based observational records starting at the end of the 19th century, indicate that the Jovian winds show high stability in latitudinal location and intensity [19, 20]. Zonal motions are dominant in Jupiter and Saturn. The mean meridional velocity, $<v>$, measured in Voyager images is typically smaller or of the same order as the errors ($\sim$ 5 - 10 ms^{-1}), so few conclusions can be drawn on meridional motions. Some authors have claimed that a correlation exists between the averaged value of the cross

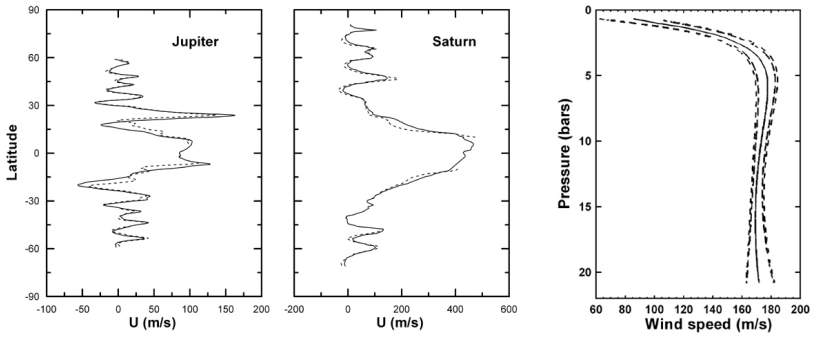

Figure 7: Left and Center: Jupiter and Saturn zonal wind profiles as determined at cloud levels around 700 mbar (continous lines) and 50 mbar (dashed lines). The 50 mbar data were derived usin eq. (2) and the temperature data from [22] and [23]. Right: Vertical wind velocity profile retrieved by the Galileo probe during its descent in 1995 in a point located at latitude 7°N [24].

products of the zonal and meridional velocity residuals $\rho<u'v'>$ and the meridional zonal shear $d<u>/dy$ [6, 21]. Here u' and v' are the velocity residuals obtained at a given latitude band, by subtracting the zonal mean velocity (averaged with respect to longitude) from the wind vector components. If this correlation exists, then the "eddies" will be transferring momentum to the jets, as in the case of the Earth's atmosphere. However, this correlation has been questioned by other authors [25]. New careful analyses of the available data (and future data for Saturn) are necessary. A calculation of the eddy heat flux $\rho C_p<v'T'>$ is also required.

Above the clouds, the measurements of the meridional temperature profile allow us to retrieve the vertical wind shear from the thermal-wind equation [26]. This relation is obtained from the momentum equation assuming hydrostatic equilibrium and geostrophic balance between the pressure gradient and the Coriolis force:

$$\frac{\partial u}{\partial z} = -\frac{g}{f R_p T}\left(\frac{\partial T}{\partial \varphi}\right)_p . \qquad (1)$$

Here z is the vertical coordinate, g the acceleration of gravity, $f = 2\Omega \sin\varphi$ the Coriolis parameter, R_p the planetary radius, T the temperature and φ the latitude. The meridional wind profile at a pressure level P above the clouds can be vertically integrated to obtain

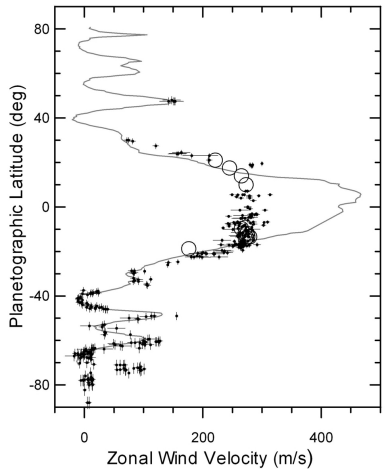

Figure 8: Saturn's wind profile in time: Continuous line from Voyagers images in 1980-81 [14], circles and dots from 1994 to 2002 using ground-based and HST images [15]

$$u_g(P) \approx u_{clouds} - \frac{g}{f}\frac{\Delta T}{TL} H \ln\left(\frac{P_{clouds}}{P}\right), \tag{2}$$

where ΔT is the difference in temperature between two latitudes separated a distance L, $H = (R_g/m)(T/g)$, is the vertical scale height (being R_g the universal gas constant and m the atmospheric molecular weight), and L is a characteristic horizontal length (e.g. the jet width). As it can be seen in Figure 7 (left), the wind jet system decreases in intensity with altitude.

Below the upper ammonia cloud, the only direct measurement of the winds was done by the Galileo probe in December 1995 which determined that the winds increased with depth from 1 to 4 bars and remained constant at least down to the level of 24 bars [24] (Figure 7, right). However, this result cannot be extrapolated to other latitudes in view of the particular meteorology of the "hot spot" area where the probe entered [27, 28].

For Saturn the number of wind vectors measured is smaller (see above) but this situation will be soon improved by the Cassini Orbiter. Figure 8 shows the zonal wind profile measured during the Voyagers flybies in 1980-81 [14] and with the HST between 1996-2003 [15]. The most conspicuous result is the apparent drop in the equatorial jet intensity during the HST period amounting to $\sim 200\ ms^{-1}$ (or 40% of the peak value). The jets outside the equator did not change and show high symmetry

with respect to the equator. The few available ground-based historical data on cloud features motions suggests that, on the long-term, the winds are stable [29]. However, the outbreak of very rare but large-scale storms, the "Great White Spots" [29] can disturb the zonal winds by injecting or extracting momentum. This is one of the possible explanations for the observed wind drop measured between 1994 to 2003 since this period follows the two GWS outbursts of 1990 and 1994 [16, 17, 30]. This aspect will be discussed later.

4 General Circulation Models

General circulation models presented to date have some common basic assumptions: (1) Spherical geometry on a planet 10 times bigger than the Earth, (2) Low viscosity and energy dissipation; (3) Rapid rotation and validity of the quasigeostrophic approximation as suggested by the low values of the Rossby number:

$$R_0 = \frac{u}{fL} < 1. \tag{3}$$

The models differ on the dominant energy source driving the motions and, consequently, on their extent in depth. We focus on two main cases: "Deep" models, that have the internal heat source as the basic energy mechanism and where motions extend along the whole hydrogen molecular layer (down to pressures of $\sim$ 1 Mbar), and "Shallow layer" models, that extend a few bars below the main upper cloud and have the solar radiation as the main energy source. In addition, we will present other proposals that assume the interplay of different energy mechanisms to produce the observed motions.

4.1 Deep circulation models

This family of models was firstly introduced for the giant planets by Busse [31]. For an inviscid and incompressible fluid confined on an spherical layer heated from below and in rapid rotation, the fluid dynamic equations show that the convective motions transporting the heat from the base to the top are subject to the constraint of the "Taylor-Proudman" theorem [32]:

$$\left(2\vec{\Omega}\cdot\nabla\right)\vec{u} = 0. \tag{4}$$

This equation states that the flow is confined to rotating columns around the rotation axis (with no vertical motions along the columns). That generates a secondary circulation in form of counter-rotating cylinders concentric with the rotation axis (Figure 9). The cylinders develop in the molecular hydrogen layer and are assumed not to penetrate the metallic hydrogen region. When the cylinders reach the

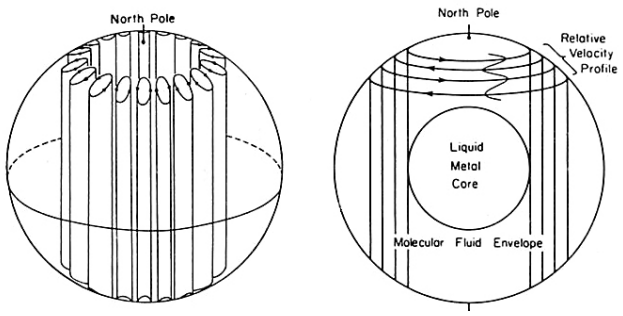

Figure 9: Scheme of the deep circulation models (columnar convection and coaxial cylindrical circulation) for the giant planets. From [13].

upper atmosphere, they give rise to the observed pattern of alternating jets. According to this hypothesis, the flow is deeply driven by the internal heat source. It extends along the whole atmosphere from one hemisphere to the other, generating a jet pattern hemispherically symmetric. The inertia of the cylinders would be so high (due to the mass they involve in the motions) that they must be very stable in time. However, if the metallic layer acts as an impenetrable barrier for the cylinders, the jet pattern should be limited in latitude by the cylinder that is tangent in the equator to the metallic region. In other words the pattern will be constrained by the width of the molecular layer (see Figure 9).

The complete set of equations that describe these motions are the continuity equation for an incompressible fluid, the Navier-Stokes equation on a rotating sphere and the thermodynamic equation:

$$\nabla \cdot \vec{u} = 0, \tag{5}$$

$$\frac{\partial u}{\partial t} + (\vec{u} \cdot \nabla)\, \vec{u} + 2\vec{\Omega} \times \vec{u} = -\frac{\nabla P}{\overline{\rho}} - \left(1 + \frac{\rho'}{\overline{\rho}}\right) \nabla \Phi + \nu \nabla^2 \vec{u}, \tag{6}$$

$$\frac{\partial T}{\partial t} + (\vec{u} \cdot \nabla)\, T = k \nabla^2 T - \left(\frac{dT}{dr}\right) \hat{k}\vec{u}, \tag{7}$$

$$\Phi = g\left(r - \frac{\Omega^2}{2g} r^2 \sin^2 \varphi\right), \tag{8}$$

being ν the kinematic viscosity, k the thermal diffusivity r the distance to the axis and $\hat{k}$ the unitary vector on the radial direction. The Boussinesq approximation is used in the continuity equation. It assumes that the fluid density is constant except

in the buoyancy term, with the temperature and density fluctuations related to their mean value by:

$$T = T + T', \tag{9}$$
$$\rho'/\overline{\rho} = -T'/\overline{T}. \tag{10}$$

The fact that the non-linear terms are small relative to Coriolis forces in the giant planets means that the Taylor-Proudman theorem remains valid. Stress-free ($u = 0$, $T = 0$) or stress-rigid ($\partial u/\partial x = 0$) are used as boundary conditions in the spherical layer. This set of equations is best studied using the classical adimensional numbers:

$$\text{Prandtl:} \quad Pr = \frac{\nu}{k}$$
$$\text{Ekman:} \quad E = \frac{\nu}{2\Omega D^2} \left(\text{or Taylor: } Ta = \frac{4}{E^2} \right)$$
$$\text{Rayleigh:} \quad Ra = \frac{g\alpha(dT/dr)D^4}{\nu k}$$

where α is the thermal expansivity and the critical Rayleigh number (Ra_{crit}) for the onset of convection depends on the Ekman number as

$$Ra_{crit} \sim E^{-4/3}.$$

The characteristic temporal scales for the diffusion processes are

$$t \approx \frac{L^2}{\nu}, \frac{L^2}{k}.$$

The equations describing the motions can then be rewritten adimensionally as

$$\nabla \cdot \vec{u} = 0, \tag{11}$$
$$E\frac{\partial u}{\partial t} + \hat{k} \times \vec{u} + \nabla P - RaET\hat{r} - E\nabla^2\vec{u} = -E\vec{u} \cdot \nabla\vec{u}, \tag{12}$$
$$\left(Pr\frac{\partial}{\partial t} - \nabla^2 \right) T - \frac{1}{r}\frac{dT}{dr}\hat{r} \cdot \vec{u} = Pr\vec{u} \cdot \nabla T. \tag{13}$$

Linear analytical solutions to this system of equations [33, 34] and, the most complete numerical solutions [35, 36, 37], show the development of the columnar modes and deep cylinder circulation as suggested by the Taylor-Proudman theorem. The main limitation of these numerical calculations relies, firstly, on the restriction for the fluid to be incompressible and, secondly, on the numerical calculations imposed

by CPU time. This restricts calculations to values of $E{>}10^{-6}$ and $Ra{<}10^{6}$ whereas for Jupiter $E{\sim}10^{-10} - 10^{-15}$ and $Ra \sim 10^{10} - 10^{15}$. In addition, it is assumed that $Pr \sim 0.01 - 10$, but indeed this parameter is not well known for Jupiter. Figure 10 shows some numerical results. The major success of these models is that they reproduce the eastward equatorial jet, showing that for high Rayleigh numbers, the kinetic energy is mainly zonal (up to 98 %) with the zonal flow driven by Reynolds stresses. The numerical models provide the Rossby number for the zonal flow and, to first order, the zonal jets have intensities $u \sim R_0 \Omega D$.

For Jupiter, using $\Omega = 1.75\text{x}10^{-4} s^{-1}$, $D \sim 10\text{x}10^{7}$ m (the depth of the hydrogen molecular layer) and $Ro \sim 0.04$ (as obtained by the numerical calculations) we get $u \sim 70$ ms^{-1} in agreement with typical Jovian flow velocities. The numerical experiments also show that quasi-columnar motions develop outside the tangent cylinder limitation imposed by the hydrogen metallic layer (Figure 11). They were also predicted by the linear approach [34], but the induced zonal motions at high latitudes have low intensities since they do not reproduce the alternating jet pattern. The numerical simulations also indicate that, when a stress-rigid boundary condition is imposed at the bottom of the atmosphere, a "multi-jet" pattern develops. In this case, however, the intensity of the wind decreases at the equator [36].

Contrary to what it could be expected, these models show that, if the convecting atmosphere has an internal statically stable layer, as suggested from calculations of the molecular hydrogen opacity in Jupiter's interior [39], the development of columnar convection can penetrate the stable layer in a phenomenon called "teleconvection" [38]. The columnar motions can propagate to the upper atmosphere and manifest themselves as a deep cylinder circulation.

A variant of the deep models that assumes the giant planet interiors to be incompressible fluids under geostrophic balance, and that pre-imposes an initial state of rotating columns (parallel to the rotation axis and traversing from one hemisphere to the other), has been recently presented [40]. The change of the column length with the distance to the rotation axis has a similar effect to the "shallow" layer β-effect (see below) in generating a turbulent pattern that evolves toward steady zonal winds. The difference with the "shallow" turbulence is that the deep "equivalent β-effect" has the opposite sign to the shallow one, and then the equatorial winds flow eastward, i. e. in the right direction. However, this model does not consider the metallic hydrogen internal region and the multi-jet pattern is not obvious in the calculations, contrarily to what the authors claim [40].

4.2 Shallow layer models

According to these models the motions are confined to the upper part of the atmospheric layer (the "troposphere"). This layer is differentially heated in latitude by the solar radiation. The meridional gradient of temperature drives the motions in a

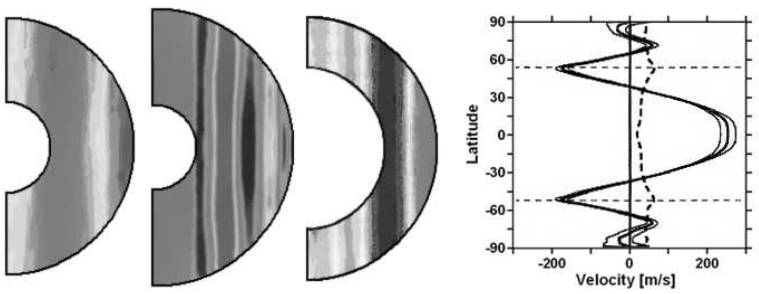

Figure 10: Numerical calculations of the columnar convection model. The figures show North-South cuts of different calculations. From left to right the following values for the adimensional numbers were used: $Pr = 1$, $E = 10^{-5}$, $Ra = 4.5 \times 10^8$ [37]; $Pr = 1$, $E = 10^{-5}$, $Ra = 10^6$ [38]; $Pr = 1$, $E = 3 \times 10^{-5}$, $Ra = 10^8$ [35]; cloud top zonal wind profile derived from the third case.

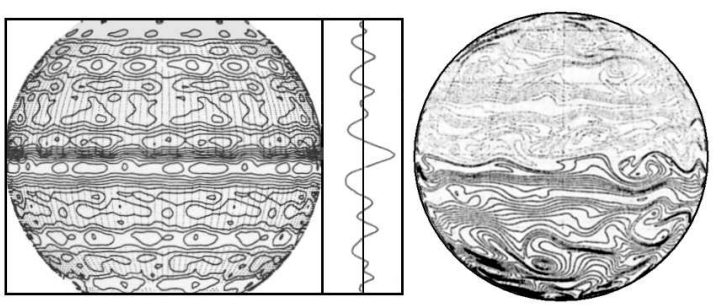

Figure 11: Shallow layer model numerical calculations. The flow field is represented by the streamlines (left) and potential vorticity (right) on the planet sphere according to calculations by two different teams [41, 42]. For the first case, an equatorially enhanced wind profile is also drawn.

frictionless (or under a weak linear drag friction) and hydrostatic quasigeostrophic balance. Williams [41, 43] was the first to formulate and solve the equations of motion for the Jovian case. In general, these models assume that an active "weather" shallow layer sits above a deep inactive "abyss". Following [42] the motions in the upper layer of this system can be rewritten as

$$\frac{\partial \vec{u}}{\partial t} + (\vec{u} \cdot \nabla)\, \vec{u} = -g\nabla h - f\hat{k} \times \vec{u} + F_a, \tag{14}$$

$$\frac{\partial h}{\partial t} + (\vec{u} \cdot \nabla)\, h = -Kh\nabla \cdot \vec{u} + F_d. \tag{15}$$

Here h is the active layer depth, F_a the adiabatic heating powering the motions and F_d a friction force [44].

Two important parameters that emerge in these models are the Rossby deformation radius, L_D, and the Rhines scale, L_β. The first represents the typical range of influence of a vortex patch on a rapidly rotating planet [20, 32]. The second represents the critical width of the zonal jets required for stability [1, 42]. They are given respectively by

$$L_D = \left(NH/f\right), \tag{16}$$

$$L_\beta = \sqrt{u/\beta}, \tag{17}$$

where $N(z)$ is the Brùnt-Väisàlä frequency, a measure of the vertical static stability of the atmosphere [26, 32]

$$N^2 = \frac{g}{T(z)}\left(\frac{dT}{dz} + \frac{g}{C_p}\right). \tag{18}$$

Given a random initial velocity, the system (14-15) is solved for h and $\vec{u}$, in order to retrieve the potential vorticity field $q(x, y)$,

$$q = \frac{\zeta + f}{h}, \tag{19}$$

$$\zeta = \hat{k}\nabla \times \vec{u}. \tag{20}$$

Here ζ is the relative vorticity and f, the Coriolis parameter, represents the planetary vorticity. Starting from a two-dimensional turbulent velocity field (the so-called "quasigeostrophic turbulence" [32]), the system evolves by means of a process known as "inverse cascade of energy" (merging the smaller scales of motion to larger structures), towards a zonally dominant jet pattern. Figure 11 shows the flow field maps for Jupiter according to this model as calculated by two different authors [41, 42].

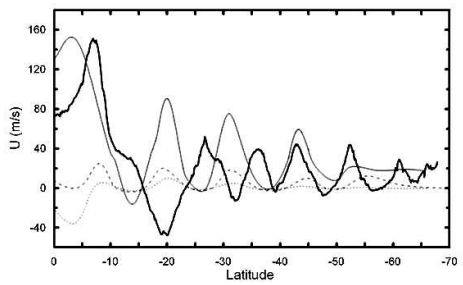

Figure 12: Zonal wind profiles at different altitudes of Jupiter according to a baroclinic intermediate "shallow" model, following [45]. Vertical levels represented are: $z = 0$ (continuous line), $z = -200km$ (dotted) and $z = -300$ km (dashed). The Voyager wind profile is also shown for comparison (thick dark line).

The main problem in these models is that the equatorial jet flows in the westward direction (opposite to that observed). To get an eastward equatorial jet, as the one seen on Figure 11 (left panel), an enhancement by an *ad hoc* forcing is needed. Recent simulations of the two-dimensional turbulence on the surface of a sphere resulting from a small-scale forcing and a large-scale drag, have shown that the flow becomes anisotropic with energy concentrated in the zonal direction [4]. The spectrum of energy density distribution has the form

$$E(n) \approx L_\beta n^{-5}, \tag{21}$$

being n the zonal wavenumber. The calculated spectrum agrees reasonably well with the observed zonal jet pattern of Jupiter and Saturn.

Advanced models that include a full baroclinic treatment of the thin hydrostatic "weather" layer for different vertical thermal structures and with a weak linear drag in the deep layer are able to reproduce the system of alternating jets and generate the equatorial superrotation in the right sense. In order to obtain these results the model requires appropriate functions for the temperature distribution in the vertical-meridional plane [45] (Figure 12). For Jupiter, the calculations indicate that the jet system extends about 200 km in depth down to $\sim$ 50 bar. One important problem of this model is that it predicts jet system to migrate in latitude as a response to the seasonal insolation cycle, but this has not been observed (see section 2). Another problem is that an unobserved equator to pole temperature difference of $10 - 20^\circ$ C must be imposed to power the jets.

It has also been proposed that in the giant planets, the "shallow" meteorologically active layer could be dynamically similar to the Earth's ocean "thermocline", an upper

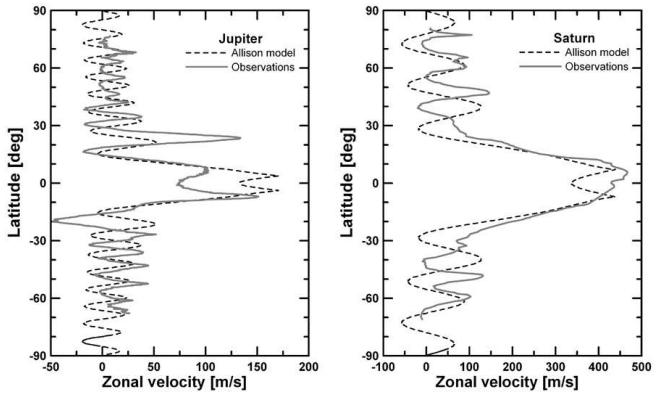

Figure 13: Zonal wind profiles (dashed lines) at cloud tops ($P \sim 0.5$ bar) in Jupiter and Saturn calculated according to the intermediate "shallow" thermocline hypothesis, as derived from [46]. They are compared to the observed profiles (continuous line).

oceanic layer of ~ 2 km depth where there is a high temperature gradient [46]. For a carefully chosen potential temperature distribution layer, an alternating zonal jet system could form down to depths ~ 50 bar in Jupiter and ~ 100 bar in Saturn. To first order, the winds should have velocities of $\sim \beta L_D^2 \cot\phi$, which amounts to $u_J \sim 130$ ms^{-1} for Jupiter and $u_S \sim 360$ ms^{-1} for Saturn (for typical values of $L_D \sim 1400$ and 3000 km respectively). The jet spacing will be then $\sim 2\pi L_D/(\sin\phi)^{1/2}$, in close agreement to that observed (Figure 13). The results are attractive but it is still to be known how this particular temperature structure is produced at those deep levels.

5 Other mechanisms that could act on the cloud level winds

Some teams have proposed that the shallow quasigeostrophic layer is bounded at its bottom by a deep but dynamically active layer that could be in solid body rotation or have a jet-like structure similar to that observed in the upper layer [47, 48]. These are "one and a half layer" models. The deep abyssal circulation corresponds to the special case $L_D = L_\beta$. Using $L_D \sim 1800$ km, as obtained from the measurements of the waves generated by the impact of the SL9 comet with Jupiter, this model predicts Jupiter's westward jets to have small variations with depth, but the eastward jets to

increase by 50-100% with depth [48]. Then the question is how these deep jets form.

An important aspect, not usually covered by these models, is the role that the magnetic field plays on the observed circulation. The magnetic field is generated by a dynamo mechanism in the inner metallic region and it may influence the deep rotating cylinders discussed in section 4.1 [49]. The toroidal magnetic field generated will produce a Lorentz force per unit mass

$$\vec{F}_L = \frac{1}{\mu_0}\left(\nabla \times \vec{B}\right) \times \vec{B} \approx \frac{R_m B^2}{4\pi\rho l}, \tag{22}$$

$$R_m = \frac{lv}{\eta(T)} \approx \frac{Hw}{\eta(T)} > 1. \tag{23}$$

Here B is the magnetic field intensity, $l \sim H$ and w are a characteristic vertical length and velocity, R_m is the magnetic Reynolds number, and $\eta(T)$ is the magnetic diffusivity. Large and broad equatorial flows could form as a result of the magnetic force [49] if it had a real effect over the upper atmosphere.

Additional external forcing on the flow can be caused by the gravitational tides raised by the massive and innermost satellites of Jupiter and Saturn [50]. For example Io produces a 116 times more intense tide than that of the Moon on the Earth, and Titan's tides on Saturn are 5 times larger than the Moon's ones on the Earth. The tides accelerate the zonal flow specially if the interior is slightly stable to convection. The calculations show that tides can accelerate the Jovian atmosphere by $\sim$ 1 cm s^{-1}/day [50]. Although this idea is suggestive, it can neither explain Saturn's equatorial flow being 5 times more intense than Jupiter's nor how the steady situation is reached.

Dynamical models that include a statically stable layer near the water clouds (above $\sim$ 6 bar in Jupiter and $\sim$ 10 bar in Saturn) have been generally successful in explaining the existence of the anticyclonic vortices. This layer extends below the penetration level of the solar radiation, and it has been argued that the increasing stability forms as a result of the latent heat release at the water clouds [51, 52] or by other thermodynamic effects (e.g. hydrogen ortho-para conversion) [53]. These thermodynamic effects could take part on the generation and maintenance of the zonal jets [54]. Moist convection can develop powerful storms transforming latent heat into intense upward motions [55] that are transformed into eddies through Coriolis forces and turbulent effects [56]. The eddies introduce momentum to the flow via a turbulent eddy flux $<\rho u'v'>$ that accelerates the jets [57]. However, the Galileo probe data indicate that the Jovian winds are not confined to the altitudes above the water cloud base at $\sim$ 6 bars, and apparently the flow is deeply rooted. Other clouds can form at much deeper levels near T = 2000 K [58]. They could have important effects over the deep dynamics stabilizing intermediate atmospheric layers and acting

as opacity sources for energy transfer. They certainly should be considered in future dynamical models.

6 Models of motions above the clouds

Different hypotheses have been suggested for the observed decrease of the wind pattern above cloud level (see section 3). One possible mechanism is that the upper flow decreases with altitude due to the friction imposed on the mean zonal flow at cloud top level. This process can be simulated by a parameterization of a dynamical balance between Coriolis forces and a Rayleigh friction drag, and by a thermodynamic balance using a Newtonian radiative damping [22, 23]. As a consequence, mass upwelling and downwelling above the clouds must occur. This motion is part of a mean meridional overturning that balances the Coriolis acceleration and the vertical advection of temperature with the dissipative effects, i.e. $fv \sim u/\tau_f$, $wHN^2/R_g \sim -\Delta T/\tau_{rad}$, where τ_f is a characteristic damping time, w the vertical velocity and τ_{rad} the radiative damping time. Another possibility is that the development of shear instabilities in the stable layer above the clouds produce large-scale eddies that give the required decay of jets within the upper troposphere and provide a physical mechanism for the underlying drag coefficient parameterization [59, 60, 61].

The dynamics in the upper troposphere and lower stratosphere is complicated by the presence of large-scale waves and by the belt-zone temperature differences produced by the differential sunlight absorption of the aerosols. The aerosols are specially abundant over the polar regions [62]. Models of the residual mean meridional circulation that take into account the solar deposition heating rates of the aerosols, result in an hemispheric-wide circulation cell (Hadley-like) that vertically extends from 1 mbar to 100 mbar [63, 64]. A two-year tracking of the aerosol debris left by the SL9 comet impact with Jupiter in 1994 supports the existence of a large meridional hemispheric circulation, but unfortunately this circulation has a sign contrary to the predictions of such models [65].

7 Laboratory Experiments

Several fluid dynamics experiments have been performed on ground and space-based laboratories aiming to simulate the general circulation on the giant planets. Many others have been done to simulate vortex formation, but these are not described here. Thermal convection experiments on a rapidly rotating sphere heated from below under microgravity conditions were performed by astronauts onboard the Spacelab [66, 67], confirming the formation of the columnar convection modes. Their experiments used $Pr = 8$, $E = 2.6 \times 10^{-3}$ and $Ra_{crit} = 2000$. Columnar motions taking place at

the onset of convection have been also observed on ground laboratories where the centrifugal force is used to compensate the gravity [34].

A deep convection laboratory analog consisting of a rotating bowl of warm water uniformly cooled at the free surface was demonstrated to generate convection cells that give rise to azimuthal jets when they encounter the free surface [68]. Symmetric bands and zonal jets in a rotating convecting fluid sphere have also been found for the following values of the characteristic numbers: $Pr = 6$, $E = 10^{-5} - 10^{-6}$ and $Ra_{crit} \sim 800$. However a low velocity equatorial jet flowing westward forms contrarily to what is observed in Jupiter and Saturn [69].

These results demonstrate that some features of the theoretical models can be captured on laboratory experiences, but new careful experiments resembling as much as possible the conditions on the giant planets interior (with respect to the values for Pr, E and Ra_{crit}) must be performed. Experiments under microgravity conditions would be specially useful (perhaps this could be an experience to develop in the International Space Station).

8 Final comments

One important point that can shed light on the general circulation is the study of the long-term temporal variability of the jet structure. A first simple argument is that if the insolation forcing dominates, as expected in most "shallow" water models, then a planet like Saturn that suffers intense seasonal insolation changes, enhanced in the equator by the ring shadowing, should follow the sunlight cycle. Its zonal jet system should change in jet location and intensity as a response to seasons. Our recent observation of a drop in Saturn's equatorial wind velocity could point in this direction [15]. However, the observed stability of the non-equatorial jets together with the scarce available historical observations of Saturn's winds suggest global long-term stability.

A second point is that we need details of the non-zonal component of the flow, including the momentum and heat transfer by eddies. In other words, we need to clarify what is the role the vortices and local motions (e. g. convective storms) play on the zonal circulation. The equatorial wind drop of Saturn could be simply the result of the large convective storm that erupted few years before the drop was detected. The change observed in the strongest jet of Jupiter [70] could have also been the result of a large disturbance that occurred there [71]. The hemispherical asymmetry observed between the tropical jets of Jupiter (compare the jets at latitudes 23°S and 23°N in Figure 6) could be due to the presence of the Great Red Spot that modifies the jets by deflecting them meridionally. If this were the case, the presence of the vortices could play an important role in shaping and pumping the jets. However, Saturn lacks in number and size the kind of large vortices present in Jupiter (at least

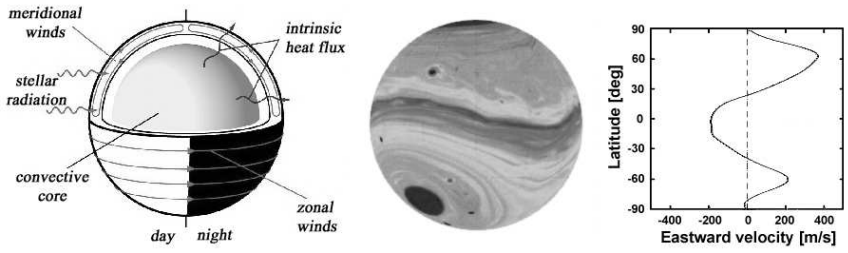

Figure 14: Proposed circulations on the extrasolar planet HD 209458b (a "hot Jupiter" class) according to the "shallow" layer hypothesis. Scheme at left is from [76]. The central sphere shows lines of potential vorticity and the plot at the right shows the derived zonal wind profile [44].

as observed at cloud level).

The stability of the jets against disturbances needs further theoretical analysis. Some westward jets are unstable according to the barotropic stability criterion [26]. The flow is stable provided that $\beta - \partial^2 < u > /\partial y^2 > 0$ at all latitudes [6]. However, other kind of stability criteria should be applied for the zonal flow if, as expected, the fluid is baroclinic [72] or deep [73]. To solve these questions we need continuous high-resolution observations of the circulation. The upcoming research by the Cassini Orbiter on Saturn, will add much data to this aspect.

New perspectives in the studies of the giant planet dynamics have been opened with the discovery of giant extrasolar planets (see reviews in [3, 11, 74, 75]). Although still at an infancy theoretical level, the variety of properties of these planets relative to those of Jupiter and Saturn with respect to their internal structure, energy sources, rotation rates, and upper clouds (see Table 1), allows the exploration of a new larger ensemble of dynamical regimes [77].

The first quantitative efforts on the development of dynamical models have been directed to the planet HD 209458b that pertains to the "hot Jupiter" family of extrasolar planets. The reason is that its properties are the best determined among all them by observations of transits in front of its central star. In particular, its radius and mass and its rotation rate, assumed to be synchronous to the orbit, have been accurately determined. Figure 14 shows the predicted flow from two simulations based on a "shallow water" model for this planet [76, 44]. These calculations show the value of comparative fluid dynamic experiments and their future application to the exploration of these new worlds.

Acknowledgements: This work has been supported by Spanish MCYT research project PNAYA2000-0932, and the Universidad del Pas Vasco Grupos grant 13697/2001. RH

thanks a post-doctoral fellowship from Gobierno Vasco. SPH acknowledges a PhD fellowship from Spanish MECD.

References

[1] Ingersoll, A.P. 1990, Science, 248, 308
[2] Ingersoll, A.P., Dowling, T.E., Gierasch, P.J., Orton, G.S., Read, P.L., Sánchez-Lavega, A., Showman, A.P., Simon-Miller, A.A., Vasavada, A.R. To appear in: Jupiter: The Planet, Satellites, and Magnetosphere (F. Bagenal, W. McKinnon and T. E. Dowling, Ed.) Cambridge University Press, (in the press)
[3] Burrows, A., Hubbard, W.B., Lunine, J.I., Liebert, J. 2001, Rev. Modern Phys. 73, 719
[4] Sukoriansky, S., Galperin, B., Dikovskaya, N. 2002, Phys. Rev. Lett., 89, 124501
[5] Hanel, R., Conrath, B., Herath, L., Kunde, V., Pirraglia, J. 1981, J. Geophys. Res., 86, 8705
[6] Ingersoll, A.P., Beebe, R.F., Mitchell, J.L., Garneau, G.W., Yagi, G.M., Muller, J.P. 1981, J. Geophys. Res., 86, 8733
[7] Limaye, S.S. 1986, Icarus, 65, 335
[8] García-Melendo, E., Sánchez-Lavega, A. 2001, Icarus, 152, 316
[9] Porco, C.C., and co-authors 2003, Science, 299, 1541
[10] Gierasch, P.J., Conrath, B.J. 1993, J. Geophys. Res., 98, 5459
[11] Guillot, T. 1999, Science, 286, 72
[12] A. R. Vasavada, A.R., Ingersoll, A.P., Banfield, D., Bell, M., Gierasch, P.J., Belton, M.J.S., Orton, G.S., Klaasen, K.P., De Jong, E., Breneman, H.H., Jones, T.J., Kaufman, J.M., Magee, K.P., Senske, D.A. 1998, Icarus, 135, 265
[13] Ingersoll, A.P., Beebe, R.F., Conrath, B.J., Hunt, G.E. 1984, Structure and dynamics of Saturn's atmosphere, in Saturn, T. Gehrels and M. S. Matthews (eds.), University of Arizona Press, Tucson, 195
[14] Sánchez-Lavega, A., Rojas, J.F., Sada, P.V. 2000, Icarus, 147, 405
[15] Sánchez-Lavega, A., Pérez-Hoyos, S., Rojas, J.F., Hueso, R., French, R.G. 2003, Nature, 423, 623
[16] Sánchez-Lavega, A., Colas, F., Lecacheux, J., Laques, P., Miyazaki, I., Parker, D. 1991, Nature, 353, 397
[17] Barnet, C.D., Beebe, R.F., Conrath, B.J. 1992, Icarus, 98, 94
[18] Sánchez-Lavega, A., Lecacheux, J., Colas, F., Laques, P. 1993, J. Geophys. Res., 98, 18857
[19] Peek, B.M. 1958, The Planet Jupiter, Faber & Faber, London
[20] Rogers, J.H. 1995, The Giant Planet Jupiter, Cambridge University Press, Cambridge
[21] Beebe, R.F., Ingersoll, A.P., Hunt, G.E., Mitchell J.L., Muller, J.P. 1980, Geophys. Res. Lett., 7, 1

[22] Gierasch, P.J., Conrath, B.J., Magalhaes, J.A. 1986, Icarus, 67, 456
[23] Conrath, B.J., Gierasch, P.J., Leroy, S.S. 1990, Icarus, 83, 255
[24] Atkinson, D.H., Pollack, J.B., Seiff, A. 1998, J. Geophys. Res., 103, 22911
[25] Sromovsky, L.A., Revercomb, H.E., Suomi, V.E., Limaye, S.S., Krauss, R.J. 1982, J. Atmos. Sci., 39, 1433
[26] Holton, J.R. 1992, An Introduction to Dynamical Meteorology, Academic Press, San Diego
[27] Showman, A.P., Ingersoll, A.P. 1998, Icarus, 132, 205
[28] Showman, A.P., Dowling, T.E. 2000, Science, 289, 1737
[29] Sánchez-Lavega, A. 1982, Icarus, 49, 1
[30] Sánchez-Lavega, A., Lecacheux, J., Gómez, J.M., Colas, F., Laques, P., Noll, K., Gilmore, D., Miyazaki, I., Parker, D. 1996, Science, 271, 631
[31] Busse, F.H. 1976, Icarus, 30, 255
[32] Pedlosky, J. 1987, Geophysical Fluid Dynamics, Second Edition, Springer-Verlag, New York
[33] Busse, F.H. 1983, Pageoph, 121, 375
[34] Busse, F.H. 1994, Chaos, 4, 123
[35] Christensen, U.R. 2001, Geophys. Res. Lett., 28, 2553
[36] Arnou, J.M., Olson, P.L. 2001, Geophys. Res. Lett., 28, 2557
[37] Christensen, U.R. 2002, J. Fluid Mech., 470, 115
[38] Zhang, K., Schubert, G. 2000, Science, 290, 1944
[39] Guillot, T., Chabrier, G., Morel, P., Gautier, D. 1994, Icarus, 112, 354
[40] Yano, J.I., Talagrand, O., Drossart, P. 2003, Nature, 421, 36
[41] Williams, G.P. 1978, J. Atmos. Sci., 35, 1399
[42] Cho, J.Y.K., Polvani, L.M. 1996, Science, 273, 335
[43] Williams, G.P. 1985, Advances in Geophysics, 28, 381
[44] Cho, J.Y.K., Menou, K., Hansen, B.S., Seager, S. 2003, ApJL, 587, L117
[45] Williams, G.P. 2003, J. Atmos. Sci., 60, 1270
[46] Allison, M. 2000, Planet Space Sci., 48, 753
[47] Ingersoll, A.P., Cuzzi, J.N. 1969, J. Atmos. Sci., 26, 981
[48] Dowling, T.E. 1995, Icarus, 117, 439
[49] Kirk, R.L., Stevenson, D.J. 1987, ApJ, 316, 836
[50] Ioannou, P.J., Lindzen, R.S. 1994, ApJ, 424, 1005
[51] Barcilon, A., Gierasch, P.J. 1970, J. Atmos. Sci., 27, 550
[52] Gierasch, P.J. 1976, Icarus, 29, 445
[53] Smith, M.D., Gierasch, P.J. 1995, Icarus, 116, 159
[54] Allison, M., Stone, P.H. 1984, Icarus, 54, 296
[55] Hueso, R., Sánchez-Lavega, A. 2001, Icarus 151, 316
[56] Hueso, R., Sánchez-Lavega, A., Guillot, T. 2002, J. Geophys. Res. Planets, 107
[57] Ingersoll, A.P., Gierasch, P.J., Banfield, D., Vasavada, A.R. 2000, Nature, 403, 630
[58] Fegley, B., Lodders, K. 1994, Icarus, 110, 117
[59] Pirraglia, J.A. 1989, Icarus, 79, 196

[60] Orsolini, Y., Leovy, C.B. 1993, Icarus, 106, 392
[61] Orsolini, Y., Leovy, C.B. 1993, Icarus, 106, 406
[62] Moses, J.I., Fouchet, T., Yelle, R.V., Friedson, A.J., Orton, G.S., Bezard, B., Drossart, P., Gladstone, G.R., Kostiuk, T., Livengood, T.A. To appear in Jupiter: The Planet, Satellites, and Magnetosphere (F. Bagenal, W. McKinnon and T. E. Dowling, Ed.) Cambridge University Press, in press.
[63] West, R.A., Friedson, A.J., Appleby, J.F. 1992, Icarus, 100, 245
[64] Moreno, F., Sedano, J. 1997, Icarus, 130, 36
[65] Sánchez Lavega, A., Gómez, J.M., Rojas, J.F., Acarreta, J.R., Lecacheux, J., Colas, F., Hueso, R., Arregu, J. 1998, Icarus, 131, 341
[66] Hart, J.E., Toomre, J., Deane, A.D., Hurlburt, N.E., Glatzmaier, G.A., Fichtl, G.H., Leslie, F., Fowlis, W.W., Gilman, P.A. 1986, Science, 234, 61
[67] Hart, J.E., Glatzmaier, G.A., Toomre, J. 1986, J. Fluid Mech., 173, 519
[68] Condie, S.A., Rhines, P.B. 1994, J. Fluid Mech., 280, 349
[69] Manneville, J.B., Olson, P. 1996, Icarus, 122, 242
[70] García-Melendo, E., Sánchez-Lavega, A., Gómez, J.M., Lecacheux, J., Colas, F., Miyazaki, I., Parker, D. 2000, Icarus, 146, 514
[71] Sánchez-Lavega, A., Miyazaki, I., Parker, D., Laques, P., Lecacheux, J. 1991, Icarus, 94, 92
[72] Dowling, T.E. 1995, Ann. Rev. Fluid Mech., 27, 293
[73] Ingersoll, A.P., Pollard, D. 1982, Icarus, 52, 62
[74] Perryman, M.A.C. 2000, Rep. Prog. Phys., 63, 1209
[75] Hubbard, W.B., Burrows, A., Lunine, J.I. 2002, ARA&A, 40, 103
[76] Showman, A.P., Guillot, T. 2002, A&A, 385, 166
[77] Sánchez Lavega, A. 2001, A&A, 377, 354